

TECHNICAL REPORT • OPEN ACCESS

The SND@LHC neutron shielding

To cite this article: D. Abbaneo *et al* 2025 *JINST* **20** T12002

View the [article online](#) for updates and enhancements.

You may also like

- [LOCALIZATION AND BROADBAND FOLLOW-UP OF THE GRAVITATIONAL-WAVE TRANSIENT GW150914](#)
B. P. Abbott, R. Abbott, T. D. Abbott et al.
- [Multi-messenger Observations of a Binary Neutron Star Merger](#)
B. P. Abbott, R. Abbott, T. D. Abbott et al.
- [The LHCb Upgrade I](#)
R. Aaij, A.S.W. Abdelmotteleb, C. Abellan Beteta et al.

TECHNICAL REPORT

The SND@LHC neutron shielding



The SND@LHC collaboration

J.A. Zamora-Saá et al.

Full author list at the end of the paper

E-mail: jilberto.zamora@unab.cl

ABSTRACT: This paper presents the design, construction, and simulation-based validation of the ColdBox, a combined neutron shielding and insulating enclosure for the Scattering and Neutrino Detector at the LHC (SND@LHC). The emulsion films in the detector's target region require protection from the intense neutron radiation background and a stable environment of 15 ± 1 °C and 50–55 % relative humidity for long-term stability. The ColdBox meets these requirements through a dual-layer structure: an external 5 cm plexiglass wall to moderate fast neutrons, and an internal 4 cm layer of borated polyethylene (with 35 % boron content) to capture thermal neutrons. The mechanical design, based on a robust aluminum frame, accommodates the constraints of the TI18 tunnel. FLUKA simulations were used to optimize the shielding configuration, showing a significant reduction in the neutron flux, with a simulated ratio of shielded to unshielded thermal neutron fluence of 2.3×10^{-3} . This result is consistent with initial measurements from BatMon detectors. The design also provides a sealed volume for a cooling system to maintain the required temperature and humidity, ensuring the necessary conditions for the emulsion films' integrity.

KEYWORDS: Overall mechanics design (support structures and materials, vibration analysis etc); Detector cooling and thermo-stabilization; Accelerator Applications; Neutrino detectors

ARXIV EPRINT: [2508.10964](https://arxiv.org/abs/2508.10964)



Contents

1	Introduction	1
2	Mechanical design and construction	2
2.1	Design requirements and frame	2
2.2	Shielding materials and Assembly	2
2.3	Sealing and safety compliance	5
2.4	Structural analysis	5
3	FLUKA simulations and shielding performance	6
3.1	Simulation setup and material selection	6
3.2	Configuration optimization and results	7
3.3	Comparison with measurements	7
4	Verification of boron content	9
5	Conclusions	9
A	ColdBox drawings	10
	The SND@LHC collaboration	16

1 Introduction

The Scattering and Neutrino Detector at the Large Hadron Collider (SND@LHC) [1] is a compact hybrid apparatus located in the T118 tunnel, 480 meters downstream from the ATLAS interaction point (IP1). It is designed to detect and distinguish the three flavors of neutrinos (ν_e , ν_μ , and ν_τ) in the high-energy regime (100 GeV–1 TeV) within the pseudo-rapidity range of $7.2 < \eta < 8.6$.

The apparatus, shown in figure 1, comprises three main subsystems. The upstream veto system identifies incoming muons from IP1. The central target region — defined for this paper as the vertex detector combined with the electromagnetic calorimeter — contains emulsion films interleaved with tungsten plates for neutrino interaction detection. The downstream muon system — defined as the hadronic calorimeter plus the muon identification system — acts as a coarse sampling calorimeter.

The emulsion films in the target region are highly sensitive to environmental conditions and radiation. For long-term stability, they require a strictly controlled environment of 15 ± 1 °C and 50–55 % relative humidity. Furthermore, they must be shielded from the intense neutron background present in the tunnel. This paper details the design, construction, and performance of a single structure, the “ColdBox”, which meets the primary requirements of a sealed environment and neutron shielding. Furthermore, the design is future-proofed with ample insulation to accommodate a cooling system, the integration and performance of which fall outside the scope of the present study.

The mechanical design was constrained by the compact and curved T118 tunnel, which features a ventilation pipe and cable trays along the wall adjacent to the detector. The design had to ensure

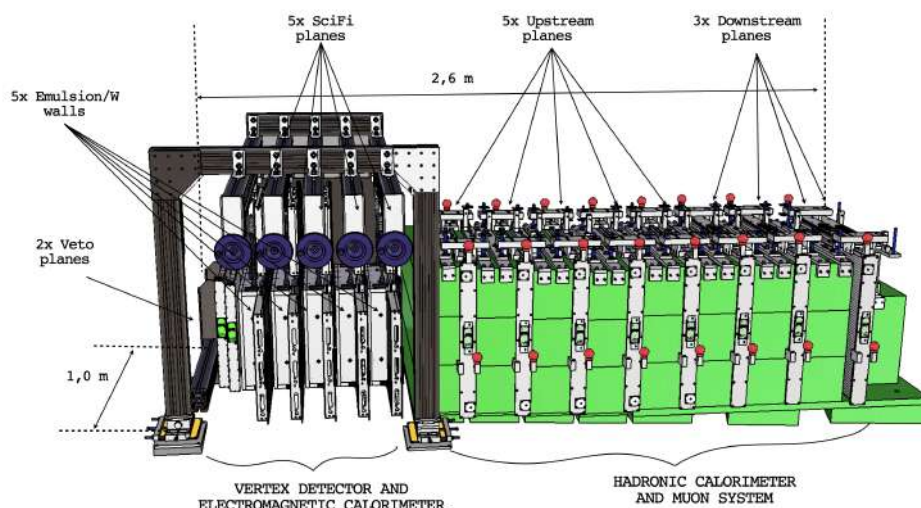


Figure 1. The SND@LHC detector.

a minimum transit aisle, provide access for an emulsion replacement trolley, and conform to the tunnel’s sloped floor. The chosen shielding strategy employs a dual-layer approach: an external moderator of plexiglass to thermalize fast neutrons, followed by an internal absorber of borated polyethylene to capture them.

This report is structured as follows: section 2 describes the mechanical design, construction, and structural analysis of the ColdBox. Section 3 presents the FLUKA simulations used to optimize the shielding configuration and assesses its performance. Section 4 verifies the material composition of the borated polyethylene. Our conclusions are given in section 5.

2 Mechanical design and construction

2.1 Design requirements and frame

The target region has an internal structure made of aluminium profiles, anchored to the floor via three feet. A primary design condition was that the ColdBox must not contact this internal structure to avoid imparting stress or movement to the detectors. The ColdBox therefore features its own self-supporting internal frame (figure 2) constructed from T-slotted aluminium profiles (specifications in table 1), designed to support the estimated 400 kg of shielding materials and four doors, each weighing approximately 150 kg. The frame was also designed to provide the necessary clearance for the emulsion replacement trolley and to host an evaporator unit on its roof (figure 3) to maintain the required internal climate within the $\sim 5 \text{ m}^3$ volume.

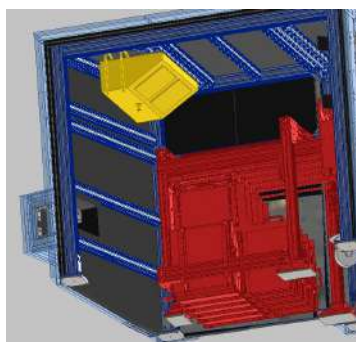
2.2 Shielding materials and Assembly

The shielding walls consist of an external 50 mm layer of plexiglass and an internal 40 mm layer of borated polyethylene. Material specifications are provided in tables 2 and 3.

The borated polyethylene (see figure 4, left side) behaves as a thermo-stable plastic similar to High-Density Polyethylene (HDPE). The two applied solutions to machine this material were water-jet cutting for rectangular contour shapes plus holes, and SPHW1204PDR-A88 WCD10 Polycrystalline

Table 1. Details of the aluminium frame.

Company	Bosch Rexroth
Material	Aluminium
Profile measures 1	80 × 80 mm ²
Profile measures 2	40 × 80 mm ²
Density	2.7 g/cm ³
Melting point	660 °C

**Figure 2.** Installed aluminium frame**Figure 3.** Evaporator highlighted in yellow over the target region highlighted in red.**Table 2.** Borated polyethylene information provided by the manufacturer.

Company	Tangyin Sanyou Engineering
Material	Borated polyethylene
Boron-carbide content	30%
Thickness	40 mm
Density	1.2g/cm ³

Table 3. Plexiglass information provided by the manufacturer.

Company	Chongqing Niubai Electromechanical
Material	Plexiglass
Thickness	50 mm
Density	1.19 g/cm ³
Melting point	175 °C
Flammable	375 °C



Figure 4. Left side: machined borated polyethylene. Right side: plexiglass sheets before the machining process.

Diamond (PCD) tool insert with 1.8 m/min of feed in a milling machine for angled contour roughing and surface roughing.

Plexiglass behaves as a thermoplastic that can be manufactured under regular conditions. Due to the significant size and required thickness, ordering two layers of 25 mm (see figure 4, right side) was necessary to reach a total of 50 mm thickness. To obtain rectangular contour shapes, the cutting method applied for this material was to use an industrial saw machine. It was also necessary to apply the drilling process for holes and angled contour roughing.

The final assembly, with overall dimensions of $2190 \times 1780 \times 1864 \text{ mm}^3$, is shown in figure 5. One wall is angled at 15° to conform to the T118 tunnel curvature. Technical drawings are provided in the appendix A.



Figure 5. View of the final ColdBox.

2.3 Sealing and safety compliance

Holes for cables, pipes, and mechanical fasteners were covered with 5 mm thick Mirrobor sheets (figure 6 left side, specifications in table 4), a flexible, boron-rich material that maintains shielding integrity (see figure 6 right side). In accordance with CERN Safety Instruction IS41 [2], which covers the use of plastics and other non-metallic materials for fire safety and radiation hardness, it was an issue to detail the specific parameters for possible ignition points for materials such as borated polyethylene because the manufacturer did not provide a proper datasheet with certified tests. For this reason, it was necessary to add an aluminium sheet of $1030 \times 815 \times 1 \text{ mm}^3$ (see figure 7) between the target region and the muon system to prevent excess heat transfer between detectors. This solution was reviewed and approved by the CERN safety team.

Table 4. Mirrobor information provided by the manufacturer.

Company	Mirrotron
Material	Mirrobor
Boron-carbide content	80 %
Thickness	5 mm
Density	1.36 g/cm^3
Melting point	$175 \text{ }^\circ\text{C}$
Flammable	$375 \text{ }^\circ\text{C}$



Figure 6. Left side: Mirrobor seals prepared to cover bolts and screws holes in the ColdBox. Right side: Mirrobor sheets before the machining process.

2.4 Structural analysis

Finite element analysis using ANSYS 2019 R1 [3] was performed to verify the structural integrity of the aluminium frame under two load scenarios: with all doors closed and with all doors open. The results, summarized in tables 5 and 6, confirm that the maximum von Mises stress and deformation are within safe limits for aluminium, with the door hinge regions identified as the most critically stressed areas.

Mirrobor (see figure 6 right side) is a rubber-like flexible material with a high boron concentration, developed by the Mirrotron manufacturer. It can be acquired in two thicknesses, 2 or 5 mm, is easy to cut by hand (with just a cutter), and is characterized as a stable, non-toxic, non-hazardous material for

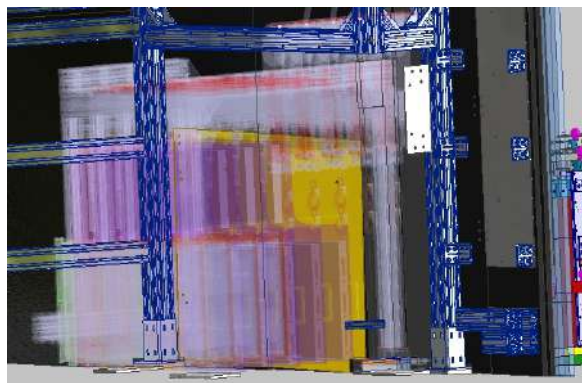


Figure 7. Aluminium sheet highlighted in yellow.

Table 5. Finite element method analysis for closed doors scenario.

Profile	80 × 80 mm
Material	Aluminium
Overall Von Mises stress	5 to 15 MPa
Maximum stress	40 MPa
Maximum deformation	0.4 mm

Table 6. Finite element method analysis for opened doors scenario.

Profile	80 × 80 mm
Material	Aluminium
Overall Von Mises stress	5 to 10 MPa
Maximum stress	86 MPa
Maximum deformation	1.1 mm

transport. However, high humidity or contact with acidic/organic solvent materials must be avoided when stored. Mirrobor was used to cover holes in the plexiglass walls.

The final design of the ColdBox has the maximum dimensions of $2190 \times 1780 \times 1864 \text{ mm}^3$ (figure 5). While the roof and the two walls that contain doors are flat and squared with frames that follow the slope of the floor. The separation between the target region and the muon system is an escalated profile, and the parallel wall that follows the TI-18 tunnel has an angle of 15° compared to the internal frame of the coldbox. Detailed drawings can be found in the appendix A.

3 FLUKA simulations and shielding performance

3.1 Simulation setup and material selection

The shielding configuration was optimized using FLUKA simulations [4, 5] with the Flair interface [6]. The simulated geometry consisted of a $2 \times 2 \times 2 \text{ m}^3$ ColdBox placed on a 0.5 m thick concrete base, with the muon system represented by an iron block (figure 8). The neutron source distribution was modeled based on one year of High-Luminosity LHC (HL-LHC) operation with an integrated luminosity of 250 fb^{-1} .

Several material combinations were explored. For the moderator, an external layer of 5 cm plexiglass was selected over high-density polyethylene due to its superior mechanical strength.¹ For the absorber, an internal layer of 4 cm borated polyethylene with 5%, 30%, and 35% boron content was evaluated; cadmium was excluded for safety reasons due to its toxicity. The 35% boron content was selected for its highest neutron capture cross-section.

¹Tensile Strength limit is 64.8–83.4 MPa for plexiglass, while for polyethylene is 11.0–43.0 MPa.

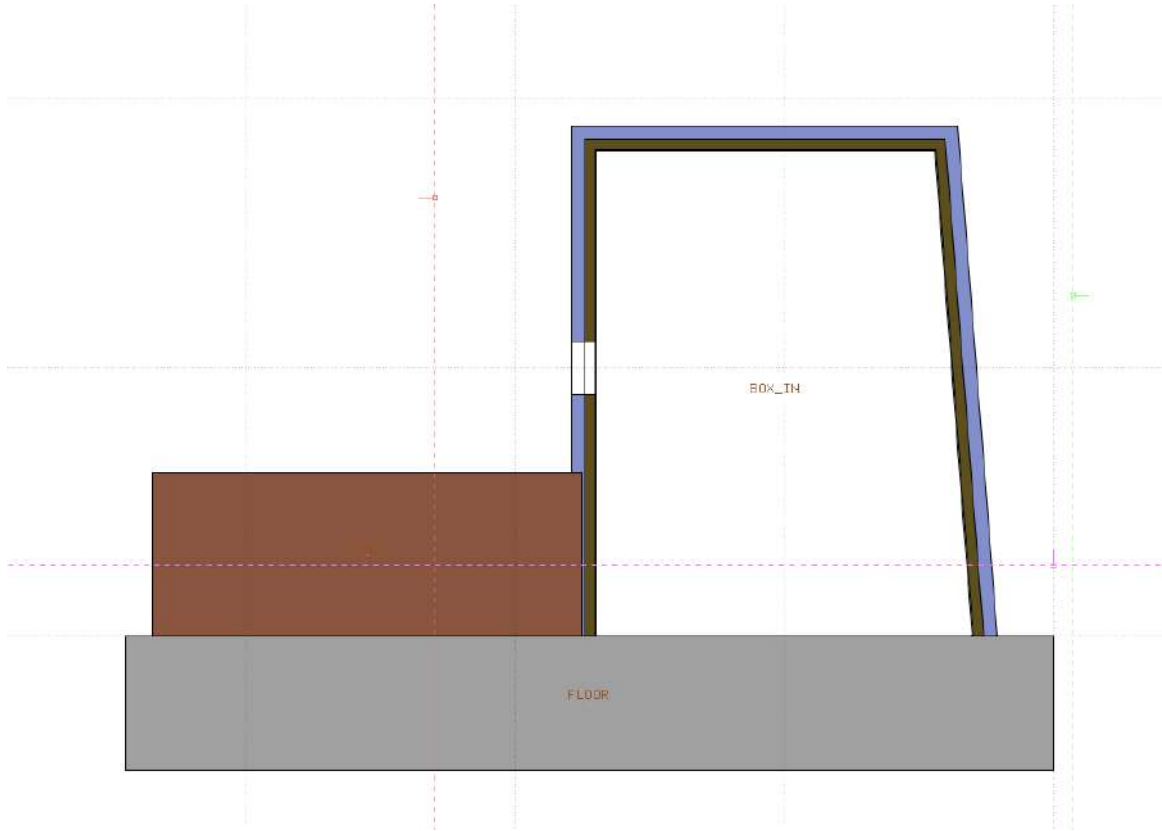


Figure 8. Lateral view of the ColdBox. The brown region represents the Muon System, the grey area represents the concrete base, the blue region represents plexiglass, and the olive region represents borated polyethylene.

3.2 Configuration optimization and results

The neutron fluence inside the ColdBox was calculated for different wall configurations (figure 9):

- *With Holes:* configurations with 5%, 30%, and 35% boron content, and holes modeling the presence of apertures for cables and pipes.
- *Without Holes:* idealized configurations with 5%, 30%, and 35% boron content, no holes were considered to isolate the effect of apertures for cables and pipes.

Figure 9 demonstrates that the chosen “Holes and 35% borated polyethylene” configuration is highly effective. The effect of the holes is negligible for thermal neutrons. The simulated ratio of neutron fluence inside the shielded ColdBox to the unshielded case, R_{SIM} , is defined as:

$$R_{SIM} = \frac{\text{Fluence with shielding (including holes)}}{\text{Fluence without shielding}}. \quad (3.1)$$

For thermal neutrons (0.025 eV), $R_{SIM} = 2.3 \times 10^{-3}$, as shown in table 7.

3.3 Comparison with measurements

The simulation results were compared with in-situ measurements from BatMon neutron monitors [7, 8]. The measured ratio, R_{BatMon} , of thermal neutron fluence inside the ColdBox (Φ_{Th}^{in}) to a location

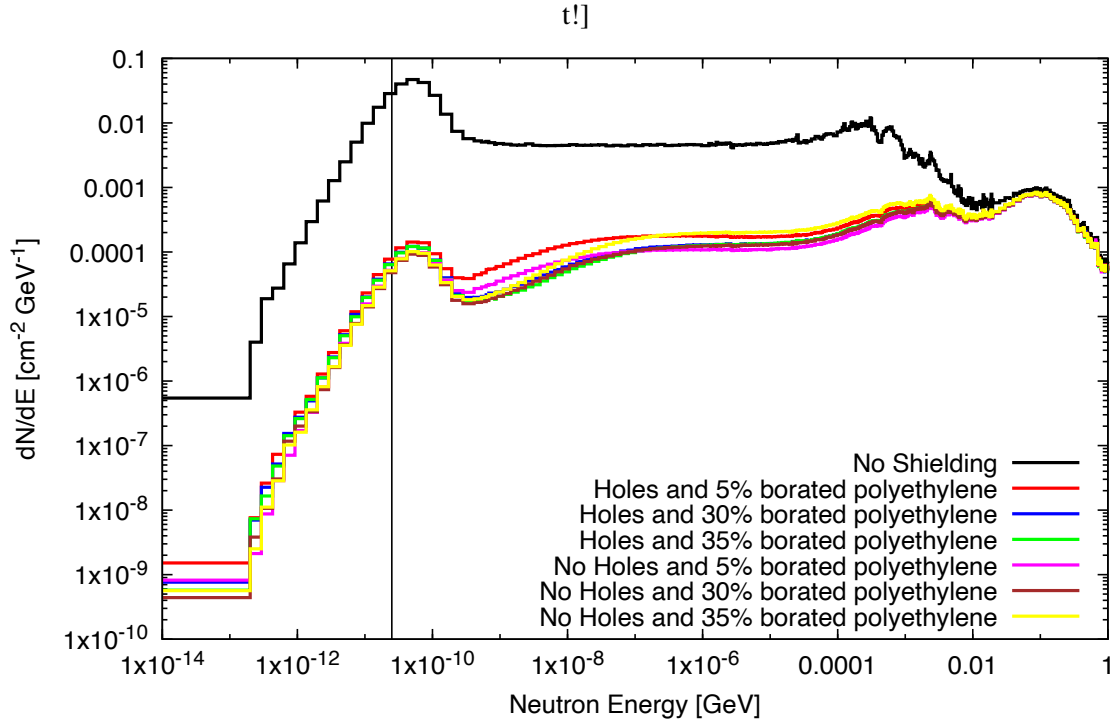


Figure 9. Neutron spectrum inside the ColdBox volume. Here 10^9 primary neutrons were simulated. The black vertical line at $E = 0.025$ (eV) stands for thermal neutrons at 20°C .

Table 7. Ratio R_{SIM} .

Neutron Energy	R_{SIM}
$= 0.025$ eV	2.3×10^{-3}
< 1 eV	2.9×10^{-3}
< 100 eV	1.6×10^{-2}
< 10 keV	2.8×10^{-2}
< 2 MeV	8.0×10^{-2}
< 20 MeV	3.0×10^{-1}
< 200 MeV	7.3×10^{-1}
< 700 MeV	7.0×10^{-1}

outside ($\Phi_{\text{Th}}^{\text{out}}$), was found to be:

$$R_{\text{BatMon}} \equiv \frac{\Phi_{\text{Th}}^{\text{in}}}{\Phi_{\text{Th}}^{\text{out}}} < \frac{2 \times 10^5 [\text{cm}^{-2} \text{s}^{-1}]}{4.40 \times 10^6 [\text{cm}^{-2} \text{s}^{-1}]} \approx 4.5 \times 10^{-2}. \quad (3.2)$$

The simulated value $R_{\text{SIM}} = 2.3 \times 10^{-3}$ is approximately a factor 20 lower than the measured upper limit.² This conservative discrepancy is expected, as the simulation includes holes that are sealed in practice with Mirrobor, and the BatMon value is an upper limit. This confirms the high efficiency

²The thermal neutron flux inside the ColdBox ($\Phi_{\text{Th}}^{\text{in}}$) was measured below the detector sensitivity ($2 \times 10^5 [\text{cm}^{-2} \text{s}^{-1}]$); therefore, we can only obtain an upper limit for the measured thermal neutron flux inside the ColdBox.

of the shielding design. In addition, Figure 9 shows that the effects of the holes (magenta, brown, and yellow lines) are not very relevant and can be neglected, particularly for energies near thermal neutron temperature.

4 Verification of boron content

To verify the boron content in the borated polyethylene, a study was conducted at the Solids Analysis Laboratory (LAS) of Andres Bello University. The results obtained are presented in table 8.

Table 8. Chemical composition of borated polyethylene was calculated using the software suite Diffrac TOPAS 4.2 [9].

Element	Weight percentage
B	35.73
C	2.11
S	2.79
O	1.60
H	0.07
Amorphous	57.69
	100.00

It is worth mentioning that in borated polyethylene, the amorphous content primarily refers to the disordered regions of the polyethylene polymer chains themselves, which are inherent to its semi-crystalline nature. This amorphous phase is crucial as it allows for the uniform dispersion and embedding of boron-based particles (like boron carbide) throughout the plastic matrix.

5 Conclusions

The design and construction of the ColdBox for the SND@LHC experiment successfully addresses the challenge of providing simultaneous neutron shielding and environmental insulation for the sensitive emulsion film target.

The selected configuration, combining a 5 cm plexiglass outer layer with a 4 cm borated polyethylene (35% boron) inner layer, was shown through FLUKA simulations to reduce the thermal neutron flux by more than two orders of magnitude ($R_{SIM} = 2.3 \times 10^{-3}$). This simulated performance is consistent with and superior to the initial upper limit established by BatMon measurements.

Mechanically, the aluminium frame provides a robust and stable support structure, with finite element analysis confirming its integrity under operational loads. The inclusion of an aluminium heat shield ensures compliance with CERN safety regulations, and the use of Mirrobor seals enhances the overall shielding effectiveness.

The ColdBox is designed to maintain a stable internal environment by providing a sealed volume for a dedicated evaporator system. Future work will focus on monitoring the long-term performance of the ColdBox, including the validation of the temperature and humidity stability during experiment operation. A more detailed analysis of shielding efficiency could be performed with more sensitive detectors capable of measuring a broader neutron energy spectrum.

A ColdBox drawings

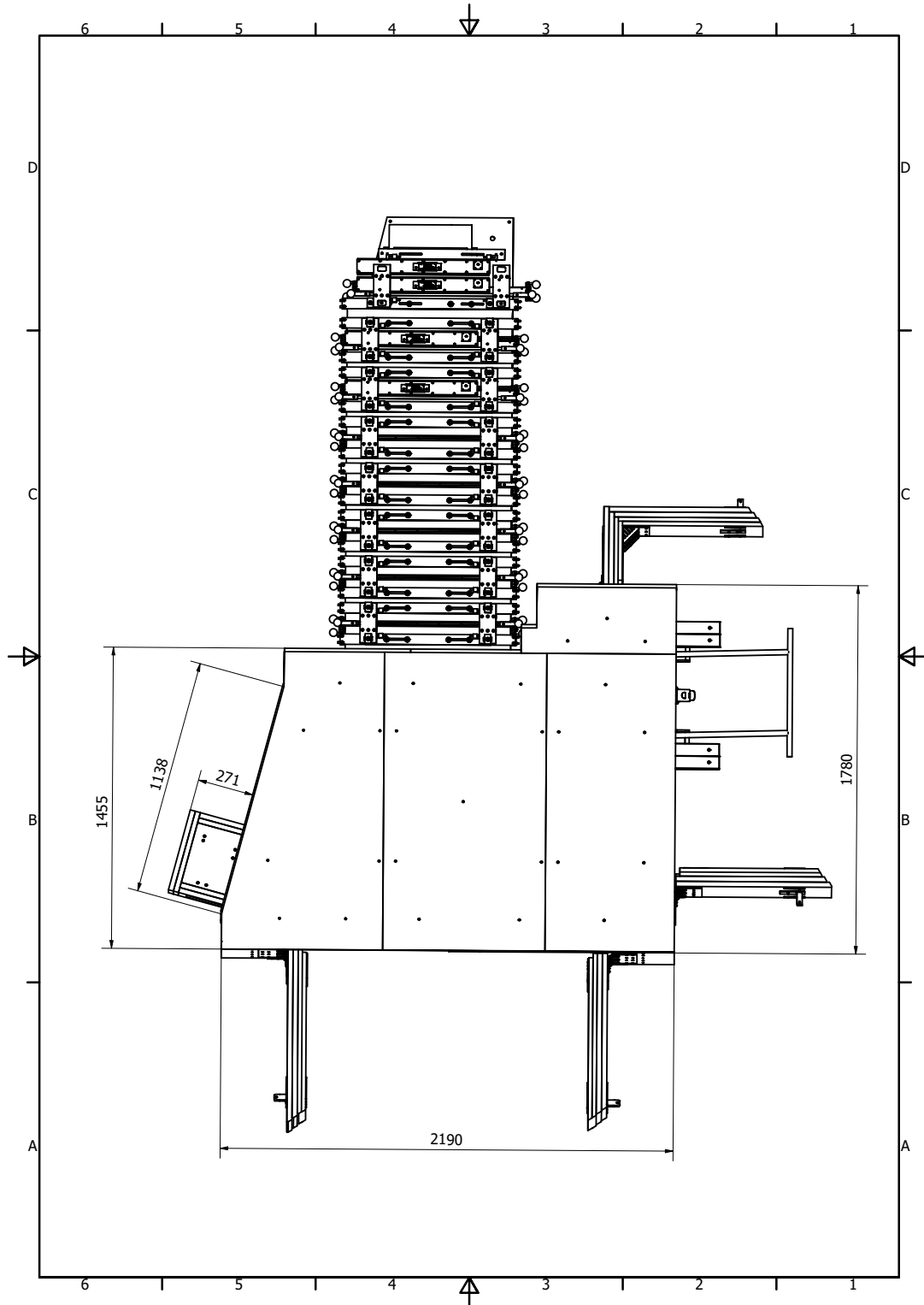


Figure 10. Top view of the ColdBox.

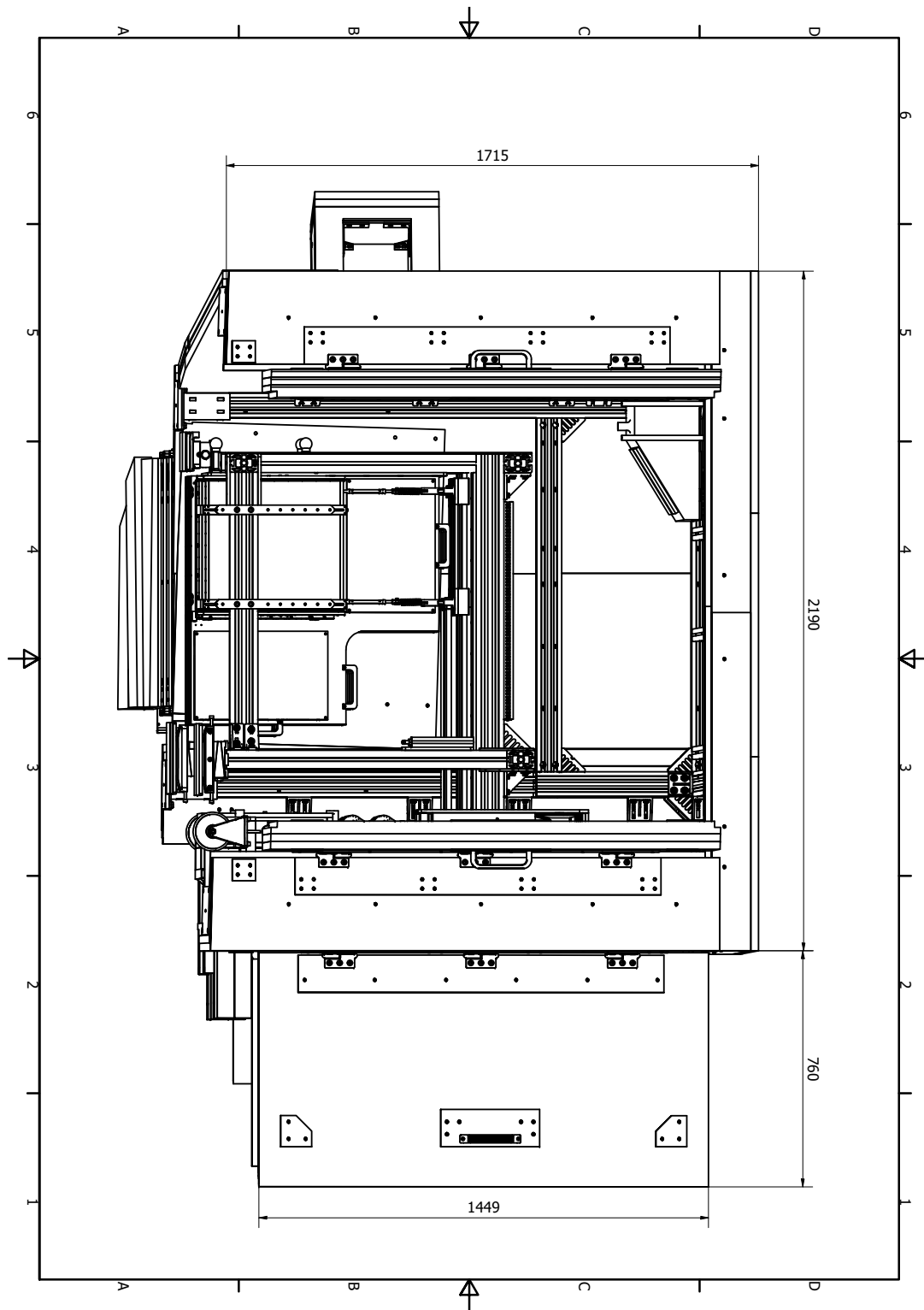


Figure 11. Front view of the ColdBox.

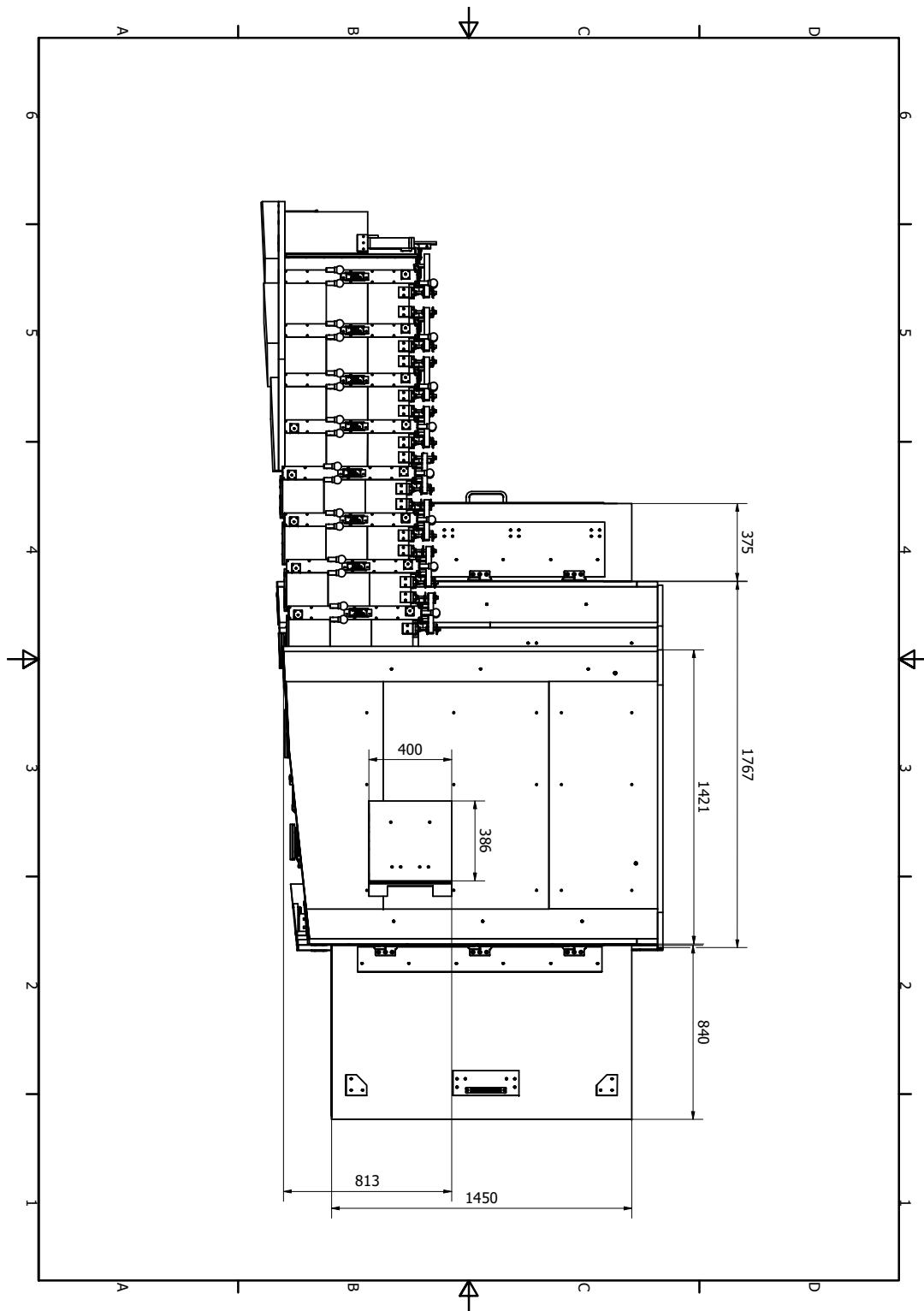


Figure 12. Left view of the ColdBox.

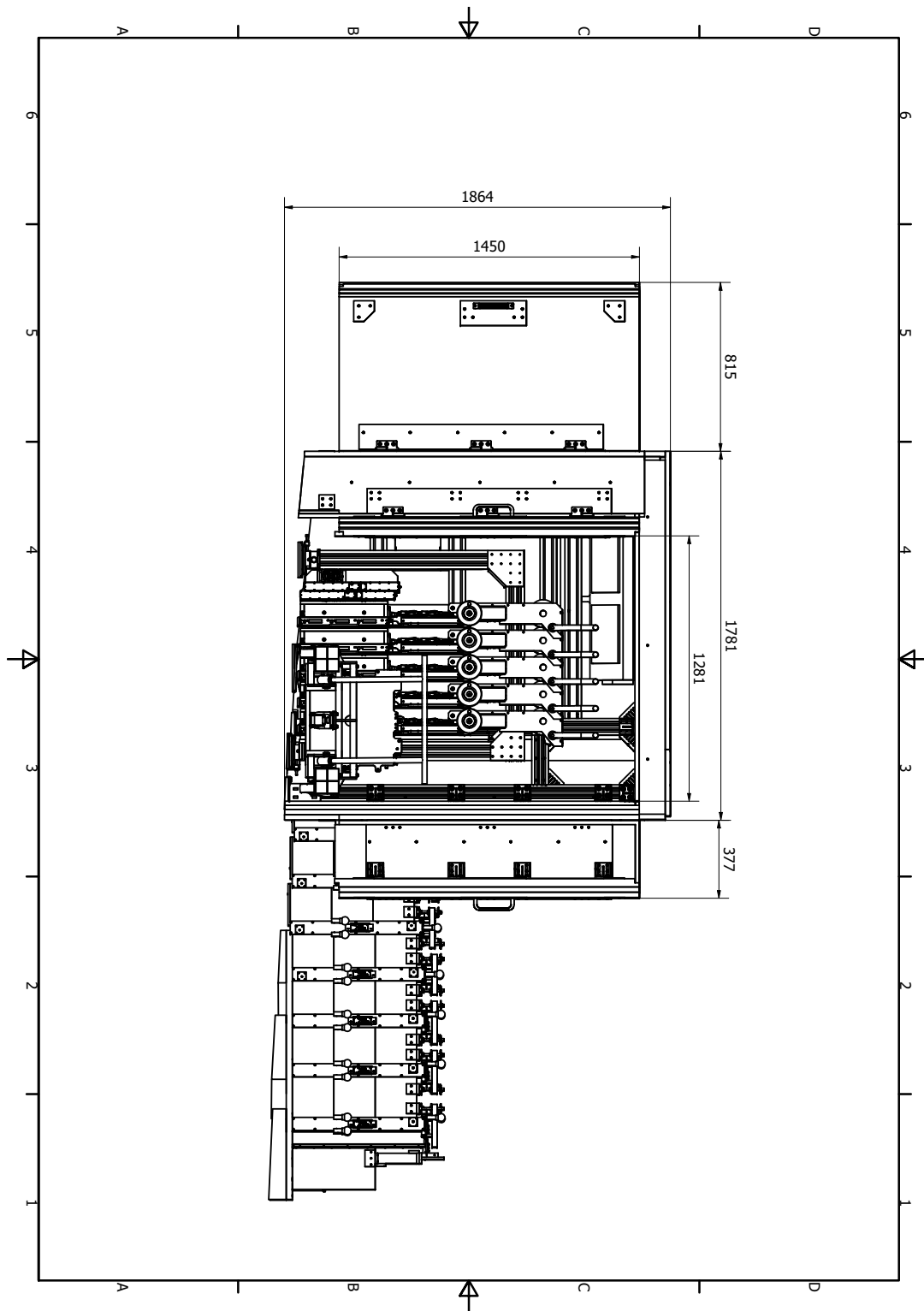


Figure 13. Right view of the ColdBox.

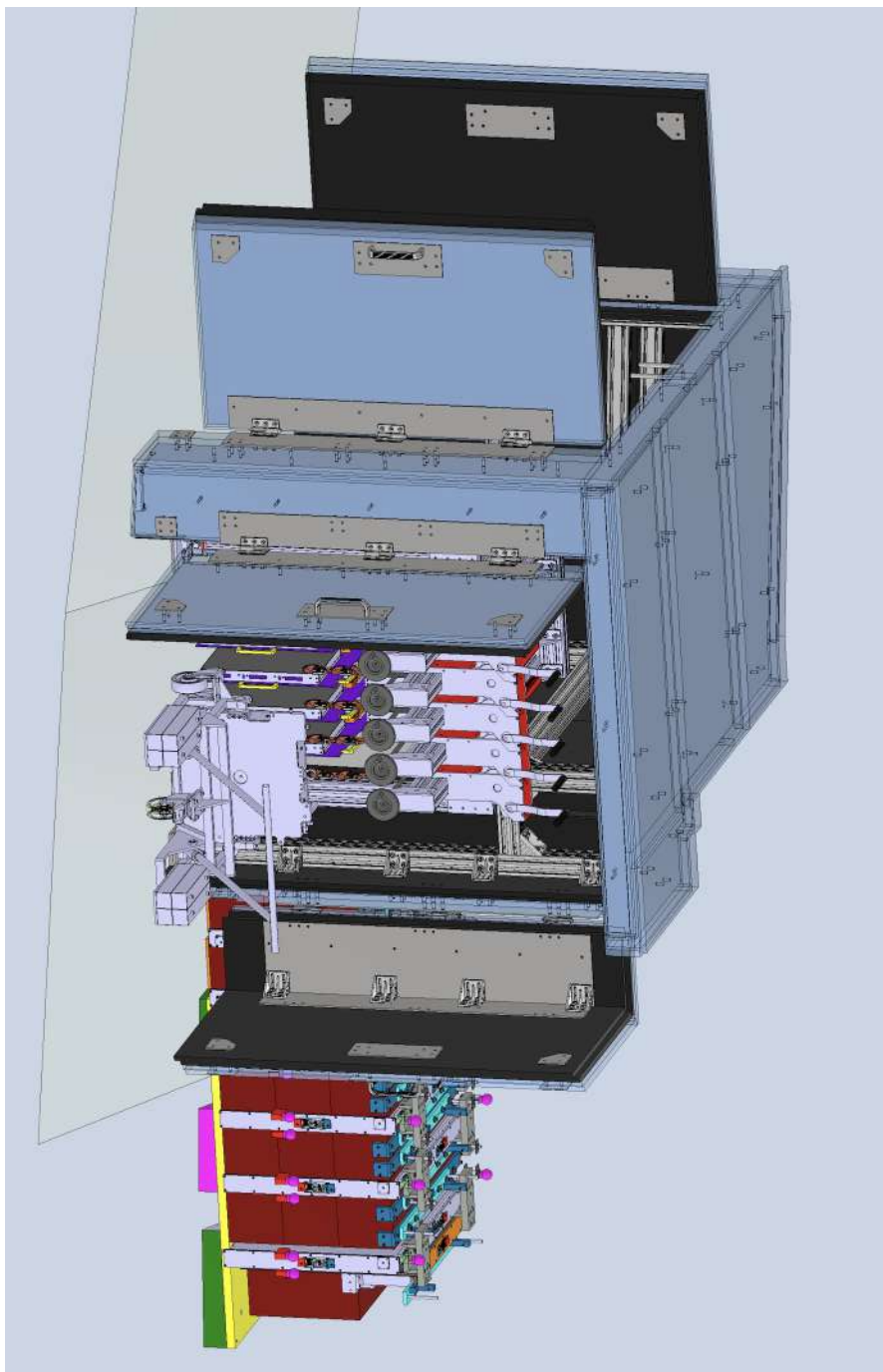


Figure 14. 3D view of the ColdBox.

Acknowledgments

We acknowledge the support for the construction and operation of the SND@LHC detector provided by the following funding agencies: CERN; the Bulgarian Ministry of Education and Science within the National Roadmap for Research Infrastructures 2020–2027 (object CERN); ANID FONDECYT grants No. 3230806, No. 1240066, 1240216 and ANID — Millennium Science Initiative Program — ICN2019_044 (Chile); the Deutsche Forschungsgemeinschaft (DFG, ID 496466340); the Italian National Institute for Nuclear Physics (INFN); JSPS, MEXT, the Global COE program of Nagoya University, the Promotion and Mutual Aid Corporation for Private Schools of Japan for Japan; the National Research Foundation of Korea with grant numbers 2021R1A2C2011003, 2020R1A2C1099546, 2021R1F1A1061717, and 2022R1A2C100505; Fundação para a Ciência e a Tecnologia, FCT (Portugal), CERN/FIS-INS/0028/2021; the Swiss National Science Foundation (SNSF); TENMAK for Turkey (Grant No. 2022TENMAK(CERN) A5.H3.F2-1). M. Climesu, H. Lacker and R. Wanke are funded by the Deutsche Forschungsgemeinschaft (DFG, German Research Foundation), Project 496466340. We acknowledge the funding of individuals by Fundação para a Ciência e a Tecnologia, FCT (Portugal) with grant numbers CEECIND/01334/2018, CEECINST/00032/2021 and PRT/BD/153351/2021. This research was financially supported by the Italian Ministry of University and Research within the Prin 2022 program.

We express our gratitude to our colleagues in the CERN accelerator departments for the excellent performance of the LHC. We thank the technical and administrative staff at CERN and at other SND@LHC institutes for their contributions to the success of the SND@LHC efforts. We thank Luis Lopes, Jakob Paul Schmidt and Maik Daniels for their help during the construction.

References

- [1] SND@LHC collaboration, *SND@LHC: the scattering and neutrino detector at the LHC*, *2024 JINST* **19** P05067 [[arXiv:2210.02784](https://arxiv.org/abs/2210.02784)].
- [2] *The use of plastic and other non-metallic materials at CERN with respect to fire safety and radiation resistance*, IS41 Rev. 1, CERN, Geneva, Switzerland (2005), https://edms.cern.ch/ui/file/335806/1.02/IS41_E.pdf.
- [3] ANSYS, Inc., *ANSYS Academic Research Mechanical*, Release 2019 R1, ANSYS, Inc. (2019), <https://www.ansys.com/products/structures/ansys-mechanical>.
- [4] C. Ahdida et al., *New Capabilities of the FLUKA Multi-Purpose Code*, *Front. Phys.* **9** (2022) 788253.
- [5] G. Battistoni et al., *Overview of the FLUKA code*, *Annals Nucl. Energy* **82** (2015) 10.
- [6] A. Donadon, G. Hugo, C. Theis and V. Vlachoudis, *FLAIR3 — recasting simulation experiences with the Advanced Interface for FLUKA and other Monte Carlo codes*, *EPJ Web Conf.* **302** (2024) 11005.
- [7] A. Zimmaro et al., *Testing and Validation Methodology for a Radiation Monitoring System for Electronics in Particle Accelerators*, *IEEE Trans. Nucl. Sci.* **69** (2022) 1642.
- [8] A. Zimmaro, S. Danzeca and S. Fiore, *Report on the 2023 BatMon measurements at the LHC and SPS*, talk given at the 57th MCWG meeting, CERN, Geneva, December 12 (2023).
- [9] Coelho-Software, *TOPAS-Academic*, V6, <http://www.topas-academic.net>.

The SND@LHC collaboration

D. Abbaneo ¹, S. Ahmad ⁴, R. Albanese ^{2,3}, A. Alexandrov ², F. Alicante ^{2,3}, F. Aloschi ¹, K. Androsov ⁵, C. Asawatangtrakuldee ⁶, M.A. Ayala Torres ^{7,8}, N. Bangaru ^{2,3}, M. Bastías Görlich ^{7,8}, C. Battilana ^{9,10}, A. Bay ⁵, A. Bertocco ^{2,3}, C. Betancourt ¹¹, D. Bick ¹², R. Biswas ¹, A. Blanco Castro ¹³, V. Boccia ^{2,3}, M. Bogomilov ¹⁴, D. Bonacorsi ^{9,10}, W.M. Bonivento ¹⁵, P. Bordalo ¹³, A. Boyarsky ^{16,17}, G. Breglio ³, S. Buontempo ², V. Cafaro ⁹, M. Campanelli ¹⁸, T. Camporesi ¹³, V. Canale ^{2,3}, D. Centanni ², S. Cepeda ^{7,8}, F. Cerutti ¹, V. Chariton ¹, K.-Y. Choi ²⁰, F. Cindolo ⁹, M. Climescu ²¹, A. Crupano ⁹, G.M. Dallavalle ⁹, N. D’Ambrosio ²², D. Davino ^{2,23}, P.T. de Bryas ⁵, R. De Asmundis ², G. De Lellis ^{2,3}, G. Del Giudice ^{2,3}, M. De Magistris ^{2,19}, A. De Roeck ¹, S. De Pasquale ²⁴, A. De Rújula ¹, D. De Simone ¹¹, H. De Souza Santos ¹³, M.A. Diaz Gutierrez ¹¹, A. Di Crescenzo ^{2,3}, C. Di Cristo ^{2,3}, D. Di Ferdinando ⁹, C. Dinc ²⁵, R. Donà ^{9,10}, O. Durhan ^{25,26}, D. Fasanella ⁹, O. Fecarotta ^{2,3}, F. Fedotovs ¹⁸, M. Ferrillo ¹¹, F. Fienga ³, A. Fiorillo ^{2,3}, R. Fresa ^{2,3}, W. Funk ¹, V. Giordano ⁹, A. Golutvin ²⁷, E. Graverini ^{5,28}, L. Guiducci ^{9,10}, A.M. Guler ²⁵, V. Guliaeva ²⁹, G.J. Haefeli ⁵, C. Hagner ¹², J.C. Helo Herrera ^{8,30}, E. van Herwijnen ²⁷, A. Iaiunese ^{2,3}, S. Ilieva ^{1,14}, S.A. Infante Cabanas ³⁰, A. Infantino ¹, A. Irace ³, A. Iuliano ^{2,3}, R. Jacobsson ¹, C. Kamiscioglu ²⁵, A.M. Kauniskangas ⁵, S.H. Kim ³¹, Y.G. Kim ³², G. Klioutchnikov ¹, M. Komatsu ³³, S. Kuleshov ^{7,8}, H.M. Lacker ³⁴, O. Lantwin ², F. Lasagni Manghi ⁹, A. Lauria ^{2,3}, K.Y. Lee ³¹, K.S. Lee ³⁵, W.-C. Lee ¹², M. Liz-Vargas ^{7,8}, V.P. Loschiavo ^{2,23}, A. Mascellani ⁵, M. Majstorovic ¹, V. Marrazzo ³, F. Mei ¹⁰, A. Miano ^{2,36}, A. Mikulenko ¹⁶, M.C. Montesi ^{2,3}, D. Morozova ^{2,3}, F.L. Navarria ^{9,10}, W. Nuntiyakul ³⁷, S. Ogawa ³⁸, M. Ovchinnikov ¹, G. Paggi ^{9,10}, A. Perrotta ⁹, R. Pinto ⁸, N. Polukhina ³⁹, F. Primavera ⁹, A. Prota ^{2,3}, A. Quercia ^{2,4}, S. Ramos ¹³, A. Reghunath ³⁴, F. Ronchetti ⁵, T. Rovelli ^{9,10}, O. Ruchayskiy ⁴⁰, T. Ruf ¹, Z. Sadykov ², V. Scalera ^{2,19}, W. Schmidt-Parzefall ¹², O. Schneider ⁵, G. Sekhniaidze ², N. Serra ¹¹, M. Shaposhnikov ⁵, T. Shchedrina ^{2,3}, L. Shchutska ⁵, H. Shibuya ^{38,41}, G. Sirri ⁹, G. Soares ¹³, J.Y. Sohn ⁴², O.J. Soto Sandoval ^{8,30}, M. Spurio ^{9,10}, J. Stegmann ⁵, D. Strelakina ^{2,3}, I. Timiryasov ⁴⁰, V. Tioukov ², C. Trippi ⁵, E. Ursov ³⁴, A. Ustyuzhanin ^{2,29}, G. Vankova-Kirilova ¹⁴, G. Vasquez ¹¹, V. Verguilov ¹⁴, N. Viegas Guerreiro Leonardo ¹³, C. Vilela ¹³, C. Visone ^{2,3}, R. Wanke ²¹, S. Yamamoto ³³, E. Yaman ^{2,3}, Z. Yang ⁵, C. Yazici ², S. Yoo ²⁰, C.S. Yoon ⁴², E. Zaffaroni ⁵, J.A. Zamora-Saá ^{7,8,*}

¹ European Organization for Nuclear Research (CERN), Geneva, 1211, Switzerland

² Sezione INFN di Napoli, Napoli, 80126, Italy

³ Università di Napoli “Federico II”, Napoli, 80126, Italy

⁴ Affiliated with Pakistan Institute of Nuclear Science and Technology (PINSTECH), Nilore, 45650, Islamabad, Pakistan

⁵ Institute of Physics, EPFL, Lausanne, 1015, Switzerland

⁶ Chulalongkorn University, Bangkok, 10330, Thailand

⁷ Center for Theoretical and Experimental Particle Physics, Facultad de Ciencias Exactas, Universidad Andrés Bello, Fernández Concha 700, Santiago, Chile

⁸ Millennium Institute for Subatomic physics at high energy frontier-SAPHIR, Santiago, 7591538, Chile

⁹ Sezione INFN di Bologna, Bologna, 40127, Italy

¹⁰ Università di Bologna, Bologna, 40127, Italy

¹¹ Physik-Institut, UZH, Zürich, 8057, Switzerland

¹² Hamburg University, Hamburg, 22761, Germany

¹³ Laboratory of Instrumentation and Experimental Particle Physics (LIP), Lisbon, 1649-003, Portugal

¹⁴ Faculty of Physics, Sofia University, Sofia, 1164, Bulgaria

¹⁵ Università degli Studi di Cagliari, Cagliari, 09124, Italy

- ¹⁶ *University of Leiden, Leiden, 2300RA, The Netherlands*
- ¹⁷ *Taras Shevchenko National University of Kyiv, Kyiv, 01033, Ukraine*
- ¹⁸ *University College London, London, WC1E6BT, United Kingdom*
- ¹⁹ *Università di Napoli Parthenope, Napoli, 80143, Italy*
- ²⁰ *Sungkyunkwan University, Suwon-si, 16419, Korea*
- ²¹ *Institut für Physik and PRISMA Cluster of Excellence, Mainz, 55099, Germany*
- ²² *Affiliated with Laboratori Nazionali del Gran Sasso, L'Aquila 67100, Italy*
- ²³ *Università del Sannio, Benevento, 82100, Italy*
- ²⁴ *Dipartimento di Fisica 'E.R. Caianello', Salerno, 84084, Italy*
- ²⁵ *Middle East Technical University (METU), Ankara, 06800, Turkey*
- ²⁶ *Also at: Atilim University, Ankara, Turkey*
- ²⁷ *Imperial College London, London, SW72AZ, United Kingdom*
- ²⁸ *Also at: Università di Pisa, Pisa, 56126, Italy*
- ²⁹ *Constructor University, Bremen, 28759, Germany*
- ³⁰ *Departamento de Física, Facultad de Ciencias, Universidad de La Serena, La Serena, 1200, Chile*
- ³¹ *Department of Physics Education and RINS, Gyeongsang National University, Jinju, 52828, Korea*
- ³² *Gwangju National University of Education, Gwangju, 61204, Korea*
- ³³ *Nagoya University, Nagoya, 464-8602, Japan*
- ³⁴ *Humboldt-Universität zu Berlin, Berlin, 12489, Germany*
- ³⁵ *Korea University, Seoul, 02841, Korea*
- ³⁶ *Affiliated with Pegaso University, Napoli, Italy*
- ³⁷ *Chiang Mai University, Chiang Mai, 50200, Thailand*
- ³⁸ *Toho University, Chiba, 274-8510, Japan*
- ³⁹ *Affiliated with JINR, Dubna, Russia*
- ⁴⁰ *Niels Bohr Institute, Copenhagen, 2100, Denmark*
- ⁴¹ *Present address: Faculty of Engineering, Kanagawa, 221-0802, Japan*
- ⁴² *Università della Basilicata, Potenza, 85100, Italy*

* *Corresponding author*